

Evaluation of VSK separation in the classification of two mineralogically different iron ore fines

Deepak Nayak, Tonmoy Kundu, Nilima Dash, Shiva Kumar I. Angadi, S.K. Chaurasiya, G.E. Sreedhar, T.V.S. Subrahmanyam, and Swagat S. Rath

Cite this article as:

Deepak Nayak, Tonmoy Kundu, Nilima Dash, Shiva Kumar I. Angadi, S.K. Chaurasiya, G.E. Sreedhar, T.V.S. Subrahmanyam, and Swagat S. Rath, Evaluation of VSK separation in the classification of two mineralogically different iron ore fines, *Int. J. Miner. Metall. Mater.*, 30(2023), No. 2, pp. 260-270. <https://doi.org/10.1007/s12613-022-2471-y>

View the article online at [SpringerLink](#) or [IJMMM Webpage](#).

Articles you may be interested in

Subhmit K. Roy, Deepak Nayak, Nilima Dash, Nikhil Dhawan, and Swagat S. Rath, [Microwave-assisted reduction roasting–magnetic separation studies of two mineralogically different low-grade iron ores](#), *Int. J. Miner. Metall. Mater.*, 27(2020), No. 11, pp. 1449-1461. <https://doi.org/10.1007/s12613-020-1992-5>

Li-xin Qian, Tie-jun Chun, Hong-ming Long, and Qing-min Meng, [Detection of the assimilation characteristics of iron ores: Dynamic resistance measurements](#), *Int. J. Miner. Metall. Mater.*, 27(2020), No. 1, pp. 18-25. <https://doi.org/10.1007/s12613-019-1869-7>

Kichakeswari Tudu, Sagar Pal, and N. R. Mandre, [Comparison of selective flocculation of low grade goethitic iron ore fines using natural and synthetic polymers and a graft copolymer](#), *Int. J. Miner. Metall. Mater.*, 25(2018), No. 5, pp. 498-504. <https://doi.org/10.1007/s12613-018-1596-5>

Xi Zhang, Shun-wei Zhu, Yu-jiang Li, Yong-li Li, Qiang Guo, and Tao Qi, [Purification of specularite by centrifugation instead of flotation to produce iron oxide red pigment](#), *Int. J. Miner. Metall. Mater.*, 28(2021), No. 1, pp. 56-65. <https://doi.org/10.1007/s12613-020-2003-6>

Wen-tao Zhou, Yue-xin Han, Yong-sheng Sun, and Yan-jun Li, [Strengthening iron enrichment and dephosphorization of high-phosphorus oolitic hematite using high-temperature pretreatment](#), *Int. J. Miner. Metall. Mater.*, 27(2020), No. 4, pp. 443-453. <https://doi.org/10.1007/s12613-019-1897-3>

Chuang Li, Chuan-yao Sun, Yu-lian Wang, Ya-feng Fu, Peng-yun Xu, and Wan-zhong Yin, [Research on new beneficiation process of low-grade magnesite using vertical roller mill](#), *Int. J. Miner. Metall. Mater.*, 27(2020), No. 4, pp. 432-442. <https://doi.org/10.1007/s12613-019-1898-2>



IJMMM WeChat



QQ author group

Evaluation of VSK separation in the classification of two mineralogically different iron ore fines

Deepak Nayak¹, Tonmoy Kundu¹, Nilima Dash¹, Shiva Kumar I. Angadi¹, S.K. Chaurasiya², G.E. Sreedhar², T.V.S. Subrahmanyam², and Swagat S. Rath¹,✉

1) Mineral Processing Department, CSIR-Institute of Minerals and Materials Technology, Bhubaneswar 751013, India

2) R&D Centre, National Mineral Development Corporation Limited, Hyderabad 500028, India

(Received: 14 January 2022; revised: 24 February 2022; accepted: 9 March 2022)

Abstract: With gradually diminishing Fe grade in tandem with the ever-increasing demand for high-grade iron ores, iron ore industries are now focusing on the beneficiation of low-grade iron ore fines, mainly considered waste. Besides, the scarcity of water at many of the mines' sites and the new water conservation policies of the governments have necessitated research on suitable dry beneficiation routes. In this context, an effort has been made to evaluate the efficacy of a dry classification unit, such as the VSK separator, in upgrading the iron values of two low-grade Indian iron ore fines, named Sample 1 and Sample 2. The mineralogical studies, involving scanning electron microscopy and X-ray diffraction, suggest that Sample 1 is a low-grade blue dust sample (51.2wt% Fe) containing hematite and quartz as the major minerals, while Sample 2 (53.3wt% Fe) shows the presence of goethite in addition to hematite and quartz. The experiments, carried out using Box–Behnken statistical design, indicate that blower speed, followed by feed rate, is the most influencing operating parameter in obtaining a good product in the VSK separator. At optimum levels of the operating factors, a fines product with ~55wt% Fe at a yield of ~40% can be obtained from Sample 1, while Sample 2 can be upgraded to ~56wt% Fe at a yield of ~85%. The results suggest that the VSK separator can be employed as an efficient intermediate unit operation in a processing circuit to upgrade the iron contents of iron ore fines.

Keywords: iron ore fines; dry beneficiation; VSK separator; Box–Behnken design

1. Introduction

India is the fourth largest iron ore-producing country after Australia, Brazil, and China. The iron ore reserves of India have been estimated to be the sixth-highest across the globe, accounting for about 5500 million tonnes [1]. However, increasing demand and extensive mining activities have resulted in the depletion of high-grade iron ore resources. Further, the revision of the cut-off grade from 58% to 45% Fe demands significant improvement in the existing technology to make the low-grade ores usable in an acceptable form for the iron and steel industries. The National Steel Policy aims to achieve a crude steel production capacity of about 300 million tonnes, by 2025–2026, to meet the national demand [2–4]. It requires processing about 590 million tonnes of high-grade ore per annum to generate a beneficiated concentrate of about 490 million tonnes, which can be further processed to meet the present goal. However, the absence of requisite high-grade resources necessitates the judicious utilization of the available low-grade iron ores. These low-grade ores are associated with high alumina and silica content, which lower the productivity of blast furnaces and pose a deleterious effect on the production cost of steel. The fine dis-

semination of such gangue impurities within the iron-bearing matrix generally demands wet processing techniques for achieving efficient separation. However, it suffers from the significant drawback of higher capital and operating expenditure than the dry route.

Extensive research has been conducted on the application of wet processing techniques for treating iron ore fines, using wet high-intensity magnetic separators, spirals, flotation, and selective flocculation [5–9]. However, the stringent environmental regulations related to increased water consumption by following the wet route, in conjunction with the additional expenditure and energy consumed for dewatering and handling the products, paves the way for exploring dry processing techniques. Dry processing increases the plant's throughput capacity and reduces the consumption of additional grinding energy by scalping fines from the downstream circuit. Dry separation technology has been comprehensively surveyed concerning the processing of iron ore fines [10–12]. Typical dry separators, which are very commonly used, include vibrating screens, air classifiers, pneumatic jigs, air tables, low- and high-intensity magnetic separators, electrostatic and electrodynamic separators. These units exploit the differences in physical properties of the valuable and gangue min-

✉ Corresponding author: Swagat S. Rath E-mail: ssrath@immt.res.in

© University of Science and Technology Beijing 2023

erals, such as particle size, density, shape, luster, magnetic susceptibility, and electrical conductivity [13]. Despite overcoming the deficits of wet processing techniques, dry unit operations are still a less lucrative option by virtue of its' poor separation efficiency [14].

Air classification is one such dry processing technique, widely followed for the separation of coarse particles from the fines, based on the differences in their settling velocities [15–17]. The first application of air classifiers dates back to the early 19th century in the cement industry [18]. Subsequently, it has found a wide range of applications in mineral processing, pharmaceutical, food, pigment, coal, and cement industries. Several researchers have reported the use of air classifiers for sizing applications [19–22]. These units are generally classified into static and dynamic types. Vane-type and V-separator operate on the principle of static air classification [23]. The absence of moving parts in static air classifiers reduces its separation efficiency and is thus gradually being replaced with the more efficient dynamic type air classifiers. The VSK separator is a typical example of a dynamic air classifier. It consists of a static V-separator coupled with a dynamic horizontal cage wheel that rotates at variable speeds to achieve better separation efficiency.

There are some reports on the use of VSK separators in the dry beneficiation of different ores and minerals. The application of the VSK separator in cement plants has been reported to significantly increase the plant's throughput capacity by reducing the recirculating load to the grinding circuit. This resulted in reduced grinding energy consumption and improved overall grinding circuit efficiency while generating a product of similar cut size. Research investigations were conducted using a VSK separator to classify and recover heavy minerals from the beach sand [24]. Literature also reports the concentration of heavy minerals and their classification by using multiple-stage VSK separators. Rougher stage VSK separator was used to classify the fines, while the cleaner stage was for the concentration of the heavy minerals [25]. A combination of High Pressure Grinding Rolls (HPGR) and air classifier reduced the grinding energy consumption considerably compared to the conventional ball mill-classifier circuit [26]. Kundu *et al.* [13] investigated the performance of the VSK separator for the classification of dolomite fines. They evaluated the effect of different operating variables, such as feed rate, cage wheel speed, and blower speed, statistically, and proposed a classification index to quantify the separation efficiency, which is simpler than conventional assessments. However, the literature on dry beneficiation of iron ore fines by VSK separator is very limited [27].

Keeping in view the above discussion, efforts have been made to evaluate the performance of the VSK separator in the classification of iron ore fines. Two iron ore fines samples, having different iron contents and mineralogical characters, have been considered in the present study. The experiments have been carried out using a statistical design approach. The research studies have a basic objective of separating the siliceous impurities from the iron-bearing minerals by varying the different operating variables at specified levels. The sig-

nificance of each variable and their interaction on the classification and separation performance has been statistically analysed. The efficiency of the VSK separator is also evaluated using the partition curves. Further, confirmatory tests have also been conducted at optimized process variables to complement the statistical analysis results.

2. Experimental

2.1. Raw materials

Two different varieties of iron ore fines were received from National Mineral Development Corporation (NMDC) Limited, Hyderabad, India. The as-received samples had a particle size of below 1 mm, and therefore, they were directly subjected to sampling by the coning and quartering method to generate the representative samples. The representative fractions were subjected to wet screening to obtain different size fractions. Size-by-size assay analysis, along with that of the test feed sample, was conducted using the wet chemical method. The mineralogical content of the representative sample was determined from the X-ray diffraction (XRD) analysis using a PANalytical, X'Pert PRO instrument in the range of 10–80° with a scanning speed of 1°/min. On the other hand, the mineral distribution and other significant textural features of the feed samples were understood from the micrographs taken using a scanning electron microscope (SEM) supplied by Zeiss (Model-EVO18).

2.2. VSK separator

The classification studies of both the iron ore samples, having a top size of –1 mm, were performed using a pilot-scale VSK separator (Model No. – SKS VS 10.4) supplied by KHD Humboldt Wedag, India. In a VSK separator, the feed material first enters the 'V' section, as illustrated in Fig. 1, through an electromagnetic feeder. At the same time, circulating air is pushed into this section in a transverse direction to the material flow so as to lift the finer fractions in between the classifying baffles to the 'SK' part. The coarser particles cascade over the baffles and get collected in the bottom discharge of the classifier. The 'SK' section consists of a cage wheel where all the fine fractions are airlifted. The air passes through the cage bars of the revolving wheel, thereby dragging all the fine particles to the center of the cage wheel for discharge to a cyclone to collect the fines. The cage wheel section of the VSK separator allows it to run at a higher feed rate without building more volume of material inside the unit as compared to the V-separator, and hence, it is a significant part of the separator.

Several design variables, such as the wheel design, wheel speed, vane angle, and vane spacing, along with other operational variables, play a vital role in the performance of the VSK separator. However, for the current investigation, specific variables such as feed rate, blower speed, and cage wheel speed were considered while other parameters were kept constant. A set of statistically designed experiments was conducted by varying the above parameters to optimize the process variables. The coarse and fines products from each

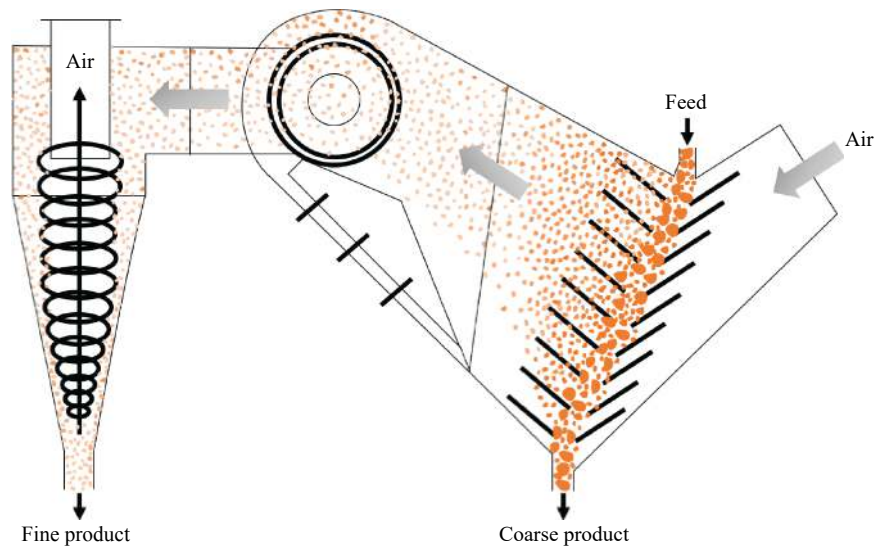


Fig. 1. Schematic illustration of the VSK separator.

experiment were weighed and subsequently subjected to wet sieving to determine the yield and cut size, respectively. Moreover, representative samples from optimized products were analyzed through chemical analysis and detailed mineralogical assessment to understand the separation process clearly.

Besides, partition curves were constructed to determine the separation efficiency of the VSK separator. The particle size analysis data of the coarse and fines products were treated as the raw data for construction of these curves. The sharpness in the gradient of these curves was considered the separation efficiency.

2.3. Experimental design

In traditional experimental design approach, only one of the studied variables is changed at a time. Therefore, the interactions of the different variables are not understood properly and the optimum processing condition is difficult to be obtained from limited rounds of experiments. Hence, response surface methodology (RSM), a factorial design approach, was considered in this work. Box–Behnken design, one of the most popular experimental design techniques using RSM, was employed to optimize the process parameters of the VSK separator. The Box–Behnken design technique has proved to be an extremely valuable tool, permitting accurate optimum values of experimental parameters and evaluating the interaction between variables with a reduced number of experiments [28–32]. The experimental data was analyzed using Design Expert 8.0 software.

The Box–Behnken design configuration for three factors, each with three levels, was chosen. The three independent variables of the separator included feed rate (A), cage wheel speed (B), and blower speed (C). Each variable was coded as -1 for low level, 0 for center level, and $+1$ for high level. The three independent variables and the assignment of their levels are described in Table 1. A total number of 18 experiments, for each of the samples, were conducted according to the design. After the experiments, the results were used to develop empirical models, which were analyzed statistically to de-

termine the influence of different factors and factor interactions on the response variables such as yield, Fe grade, and d_{50} . It may be noted that the d_{50} cut size is the particle size, at which 50wt% of the particles report either to the coarse or fines product. Besides, the data were analyzed, using ANOVA (Analysis of Variance), to rank the factors and interaction as per their significance in the process. Further, a response surface analysis was performed to predict the optimal conditions, and subsequently, confirmation tests were conducted to check the accuracy of the models developed.

Table 1. List of independent variables and their corresponding levels

Variables	Unit	Code name	Levels		
			-1	0	$+1$
Feed rate	kg/min	A	600	1200	1800
Cage wheel speed	r/min	B	480	780	1080
Blower speed	r/min	C	25	35	45

3. Results and discussion

3.1. Feed characterization

The two samples, received from NMDC Ltd., were distinctly different in appearance even though both of them had a top particle size of 1 mm. One of them had deep bluish black color while the other looked brown. They were named Sample 1 and Sample 2, respectively. The megascopic images of both the samples are displayed in Fig. 2.

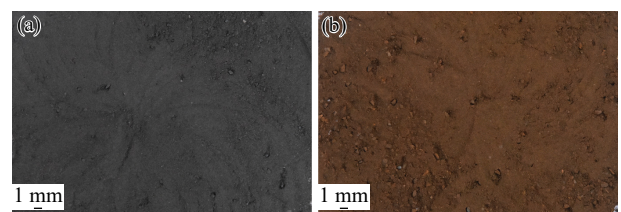


Fig. 2. Photographs of iron ore fines: (a) Sample 1 and (b) Sample 2.

The results of the wet-chemical analysis of Sample 1 are given in Table 2. The feed material contains around 51wt% Fe, 26wt% SiO₂, and other minor elements. The size analysis data indicates that the feed includes approximately 32wt% by weight the ultrafine fraction (<38 µm), having an iron content of about 57wt% and a silica content of about 16wt%. The calculated results from the size analysis of the Sample 1 feed reveal that the undersize fraction resulting from the classification at a cut-size of 53 µm could be an iron-rich product with low silica content (Table 3). Considering 100% separation efficiency at a cut-size of 53 µm, a product having Fe content over 55wt% with a yield of about 42% could be obtained.

Similarly, the wet-chemical analysis of the Sample 2 feed reveals that it contains around 53wt% Fe and 20wt% SiO₂ (Table 4). The size analyses and size-wise chemical analyses of the feed are also given in Table 4. In this case, the size analysis indicates that the feed contains around 26wt% by weight of the ultrafine fraction (<38 µm), having an iron content of about 43wt% and a high silica content of about 34wt%. Moreover, it can be inferred from the calculated results (Table 5) that a size classification at 45 µm could separate around 28wt% by weight of fines having a higher content of impurities (~32wt% SiO₂ and 2wt% Al₂O₃). As a result, a

Table 2. Size analysis and size-wise chemical analysis of the feed of iron ore Sample 1

Size / µm	Weight / wt%	Assay / wt%			
		Fe	Al ₂ O ₃	SiO ₂	LOI
+850	1.51	53.31	2.04	21.65	0.29
-850+600	4.35	56.12	1.02	15.67	0.40
-600+425	3.84	57.52	1.02	14.87	0.47
-425+300	4.14	49.14	1.53	26.89	0.32
-300+212	3.88	39.64	1.27	40.82	0.40
-212+150	5.20	40.01	1.02	41.34	0.28
-150+106	8.46	36.29	1.02	46.41	0.27
-106+75	8.52	39.22	1.78	40.21	0.23
-75+53	17.78	51.66	1.53	23.20	0.27
-53+45	2.93	45.34	2.04	22.05	0.33
-45+38	7.21	52.66	1.53	22.15	0.25
-38	32.19	57.24	1.02	15.86	0.39
Calculated head	100.00	50.25	1.29	25.25	0.33
Actual head		51.38	1.15	26.41	0.60

Note: LOI—Loss on ignition.

coarse product with a yield of about 72%, an iron content of about 56wt%, and a silica content of about 17wt% could be produced, assuming 100% separation efficiency for a cut-size of 45 µm.

Table 3. Size-wise weight and elemental distribution calculated for classification of the feed of iron ore Sample 1 at 53 µm

Size / µm	Weight / wt%	Assay / wt%				Distribution / wt%			
		Fe	Al ₂ O ₃	SiO ₂	LOI	Fe	Al ₂ O ₃	SiO ₂	LOI
+53	57.67	46.30	1.37	31.04	0.30	53.14	61.31	70.90	53.11
-53	42.33	55.63	1.18	17.36	0.36	46.86	38.69	29.10	46.89
Calculated head	100.00	50.25	1.29	25.25	0.33	100.00	100.00	100.00	100.00

The backscattered electron images, observed under SEM (Fig. 3), show the distribution of mineral and gangue particles in both the iron ore samples. In Sample 1, the coarser fractions consisting of +53 µm size particles contain more quartz (Fig. 3(a)) as compared to its finer fraction (Fig. 3(b)). In other words, the finer fractions of the Sample 1 contain a higher amount of liberated hematite particles. While most quartz phases are found as subhedral to anhedral grains of various sizes, the hematite minerals are observed as disseminated grains showing salt and pepper texture. On the other hand, the coarser fractions (+45 µm size) of Sample 2 contain comparatively more locked or unliberated mineral and gangue particles (Fig. 3(c)). The hematite and goethite minerals could be seen as inclusions in the phenocrysts of quartz phases. At places, hematite and goethite phases, varying in shape and size, are also intricately associated with the quartz matrix. The finer fractions of the Sample 2 primarily consist of liberated gangue particles in the form of quartz phases, along with some sparsely and independently distributed iron phases (Fig. 3(d)).

The observations under SEM were also correlated with the mineral phases interpreted from the XRD patterns of both the feed samples (Fig. 4). As seen from the XRD pattern of the

coarser fraction of the Sample 1 (Fig. 4(a)), it primarily consists of quartz with some amounts of hematite. However, the finer fractions of the feed are mainly composed of hematite

Table 4. Size analysis and size-wise chemical analysis of the feed of iron ore Sample 2

Size / µm	Weight / wt%	Assay / wt%			
		Fe	Al ₂ O ₃	SiO ₂	LOI
+850	11.96	52.49	1.02	21.97	1.70
-850+600	10.93	51.94	1.02	22.01	1.70
-600+425	6.96	51.38	1.78	22.30	1.80
-425+300	6.18	51.94	1.27	22.01	1.80
-300+212	4.40	57.20	1.27	14.80	1.90
-212+150	4.69	60.87	1.78	9.60	1.80
-150+106	7.00	59.75	1.53	10.30	1.60
-106+75	5.76	62.55	1.02	8.17	1.60
-75+53	9.23	63.11	0.59	7.40	1.40
-53+45	4.44	54.73	0.80	19.40	1.50
-45+38	2.53	55.29	1.27	19.25	1.40
-38	25.91	43.00	1.78	33.70	3.10
Calculated head	100.00	52.70	1.32	21.00	2.03
Actual head		53.27	1.27	20.30	2.10

Table 5. Size-wise weight and elemental distribution calculated for classification of the feed of iron ore Sample 2 at 45 μm

Size / μm	Weight / wt%	Assay / wt%				Distribution / wt%			
		Fe	Al ₂ O ₃	SiO ₂	LOI	Fe	Al ₂ O ₃	SiO ₂	LOI
+45	71.56	56.12	1.16	16.47	1.67	76.2	62.7	56.1	58.7
-45	28.44	44.09	1.73	32.42	2.95	23.8	37.3	43.9	41.3
Calculated head	100.00	52.70	1.32	21.00	2.03	100.00	100.00	100.00	100.00

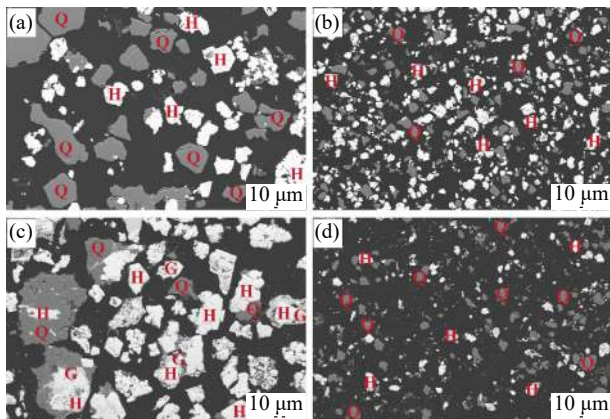


Fig. 3. SEM backscattered image of (a) Sample 1 (+53 μm size), (b) Sample 1 (-53 μm size), (c) Sample 2 (+45 μm size), and (d) Sample 2 (-45 μm size). H: hematite, Q: quartz, and G: goethite.

with a moderate amount of quartz (Fig. 4(b)). Similarly, the XRD pattern of the Sample 2 coarser fractions confirms the presence of hematite and goethite as the iron minerals

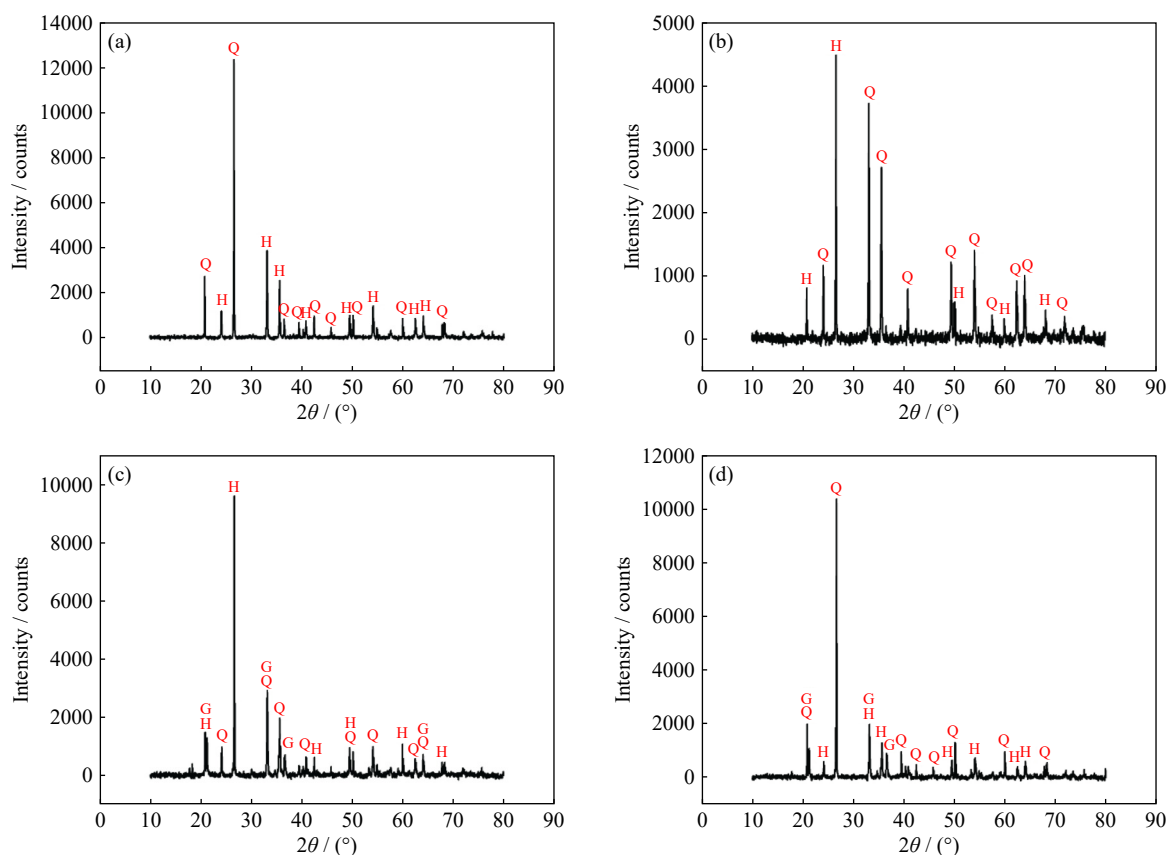


Fig. 4. XRD patterns of (a) Sample 1 (+53 μm size), (b) Sample 1 (-53 μm size), (c) Sample 2 (+45 μm size), and (d) Sample 2 (-45 μm size). H: hematite, Q: quartz, and G: goethite.

(Fig. 4(c)). The gangue mineral is mainly represented by quartz. Conversely, quartz is found as the dominant mineral in the finer fractions of sample feed 2 (Fig. 4(d)). Overall, the test feed's characterization studies reveal that a separation of a finer fraction of Sample 1 at a cut-size of 53 μm , while that of a coarser fraction of Sample 2 at a cut-size of 45 μm could yield iron-rich products.

3.2. Statistical analysis and optimization of process variables

As presented in the previous sections, the size analyses and mineralogical data indicate that the two iron ore samples are very different from each other. Sample 1 has more Fe values in the fines, while the coarse fractions of Sample 2 are Fe rich. Therefore, it is evident that a size classification of the two samples would lead to Fe enrichment in both the samples. But, the major difference is that the undersize fraction will be a product in the case of Sample 1, whereas the coarse fraction will be a product in the case of Sample 2. The results of the VSK separator experiments, carried out according to the statistical design, are presented in Table 6 in terms

of yield (%), Fe content (wt%), and d_{50} (μm).

The results suggest that the upgradation in Fe content, in the case of both the samples, is limited to 3%–5%. In contrast, there is a wide variation in the yield values. The operating parameters, namely, feed rate, cage wheel speed, and blower speed, appear to be influencing the yield values more than they affect Fe grade. The other response, d_{50} , considered in this study, is directly related to yield.

The data displayed in Table 6 were used to develop best fit models for the three responses as functions of the factors listed in Table 1. The models designed for Sample 1 are given

in Eqs. (1)–(3), while those for Sample 2 are presented in Eqs. (4)–(6).

$$\text{Yield} = 36.70 - 11.00A - 0.40B + 12.83C + 6.31AB - 5.04AC - 1.09BC - 4.54A^2 + 3.98B^2 + 4.34C^2 \quad (1)$$

$$\text{Fe content} = 54.49 + 0.18A + 0.70B - 1.05C - 0.26AB + 0.033AC - 0.045BC + 0.20A^2 + 0.027B^2 - 1.14C^2 \quad (2)$$

$$d_{50} = 51.34 - 17.52A - 3.74B + 20.27C + 13.61AB - 11.71AC - 3.13BC \quad (3)$$

Table 6. Box–Behnken design matrix showing the details of the tests performed and the respective responses

Sample 1						
No.	Factor 1	Factor 2	Factor 3	Response 1	Response 2	Response 3
	<i>A</i>	<i>B</i>	<i>C</i>	Yield / %	Fe content / wt%	d_{50} / μm
1	600	480	35	56.7	53.3	90.7
2	1800	480	35	24.5	53.5	32.9
3	600	1080	35	35.2	56.1	37.6
4	1800	1080	35	28.2	55.3	35.4
5	600	780	25	30.6	54.0	37.3
6	1800	780	25	16.3	55.0	20.0
7	600	780	45	66.8	51.7	99.0
8	1800	780	45	32.3	52.8	35.0
9	1200	480	25	27.7	53.7	33.5
10	1200	1080	25	37.1	55.0	49.5
11	1200	480	45	55.1	52.6	79.9
12	1200	1080	45	60.2	52.2	85.9
13	1200	780	35	36.7	54.5	47.4
14	1200	780	35	36.8	54.3	47.8
15	1200	780	35	36.9	54.2	48.2
16	1200	780	35	36.5	54.8	46.9
17	1200	780	35	36.6	54.7	48.5
18	1200	780	35	36.7	54.5	47.5

Sample 2						
No.	Factor 1	Factor 2	Factor 3	Response 1	Response 2	Response 3
	<i>A</i>	<i>B</i>	<i>C</i>	Yield / %	Fe content / wt%	d_{50} / μm
1	600	480	35	55.1	56.8	103.5
2	1800	480	35	77.9	55.9	55.5
3	600	1080	35	77.2	56.1	52.5
4	1800	1080	35	76.2	56.4	47.4
5	600	780	25	79.1	54.9	51.5
6	1800	780	25	87.0	55.3	20.0
7	600	780	45	52.3	55.3	105.1
8	1800	780	45	68.0	54.7	53.7
9	1200	480	25	81.1	56.3	35.8
10	1200	1080	25	82.4	56.4	36.4
11	1200	480	45	56.9	55.9	98.4
12	1200	1080	45	56.8	55.0	101.3
13	1200	780	35	66.6	55.9	81.4
14	1200	780	35	66.8	55.3	82.8
15	1200	780	35	66.2	56.1	83.1
16	1200	780	35	66.6	55.8	81.4
17	1200	780	35	66.7	55.4	81.2
18	1200	780	35	66.5	55.9	81.9

$$\text{Yield} = 66.56 + 5.67A + 2.68B - 11.95C - 5.96AB + 1.94AC - 0.34BC + 3.64A^2 + 1.38B^2 + 1.38C^2 \quad (4)$$

$$\text{Fe content} = 55.72 - 0.10A - 0.11B - 0.24C + 0.31AB - 0.25AC - 0.25BC - 0.13A^2 + 0.71B^2 - 0.55C^2 \quad (5)$$

$$d_{50} = 81.97 - 17.00A - 6.95B + 26.85C + 10.73AB - 4.93AC + 0.57BC - 13.82A^2 - 3.42B^2 - 10.57C^2 \quad (6)$$

The models were selected based on the ANOVA tables generated, using the statistical package. Some key statistical parameters that signify the goodness of fit of the models are presented in Table 7. A Model F value of 17.33%, for the yield of Sample 1, suggests that it is a good fit having a probability of only 0.0002 for noise being responsible for this Model F value. A similar explanation can be given for the rest of the models developed. The high R^2 values, obtained in most of the models, substantiate the corresponding high Model F values. Adequate precision, another statistical parameter calculated and presented in Table 7, is the signal-to-noise ratio, which is a comparison of the range of the predicted values at the design points to the average prediction error. The precision of more than 4 for all the developed models indicates that the models can be used to navigate the design space. To confirm the adequacy of the developed models, the model-predicted values for different responses were compared with the actual experimental data. Fig. 5, showing the predicted vs. actual plots for all the responses for both the samples, indicates a reasonable agreement between

the experiments and the models developed for all the responses.

The signs associated with the terms (factors and interactions) in Eqs. (1)–(6), indicate whether the corresponding term impacts the model response positively or negatively. The positive sign for the coefficients indicates that the response would increase with the increase of the value of term, while the negative sign suggests the decrease of the response with the increase in that term [33]. The relative significance of the terms can be ascertained from the corresponding F values. The higher the F value, the more significant the term is.

As shown in Fig. 6, for Sample 1, C (blower speed) is the most significant term for all three responses. In the case of yield and d_{50} , the next important term is A (feed rate). It is interesting to observe that B (cage wheel speed) has minimal effect on the two responses. However, B is one of the most significant terms for the response Fe content. The effect of the other terms like AB , AC , BC , A^2 , B^2 , and C^2 are relatively less significant for all the three responses of Sample 1, with an exception for Fe content, where C^2 is the 2nd most important term after C .

In the case of Sample 2, the effects of the factors are not similar to that for Sample 1. Though C continues to be the most significant term for yield (%) and d_{50} , B^2 followed by C^2 is the topmost important term for Fe content (wt%). The effect of other terms like AB , AC , BC , A^2 , B^2 , and C^2 are relatively less significant in the case of yield (%) and d_{50} , but not

Table 7. Various statistical parameters of all the models developed

Statistical parameter	Sample 1			Sample 2		
	Yield / %	Fe content / wt%	d_{50} / μm	Yield / %	Fe content / wt%	d_{50} / μm
Model F value	17.33	5.89	9.76	31.19	4.72	11.72
p value (Prob > F)	<0.0002	<0.0101	<0.0007	<0.0001	<0.0198	<0.0010
R^2	0.9512	0.8688	0.8419	0.9723	0.8415	0.9295
Adeq precision	15.148	7.687	11.134	19.208	9.470	11.722

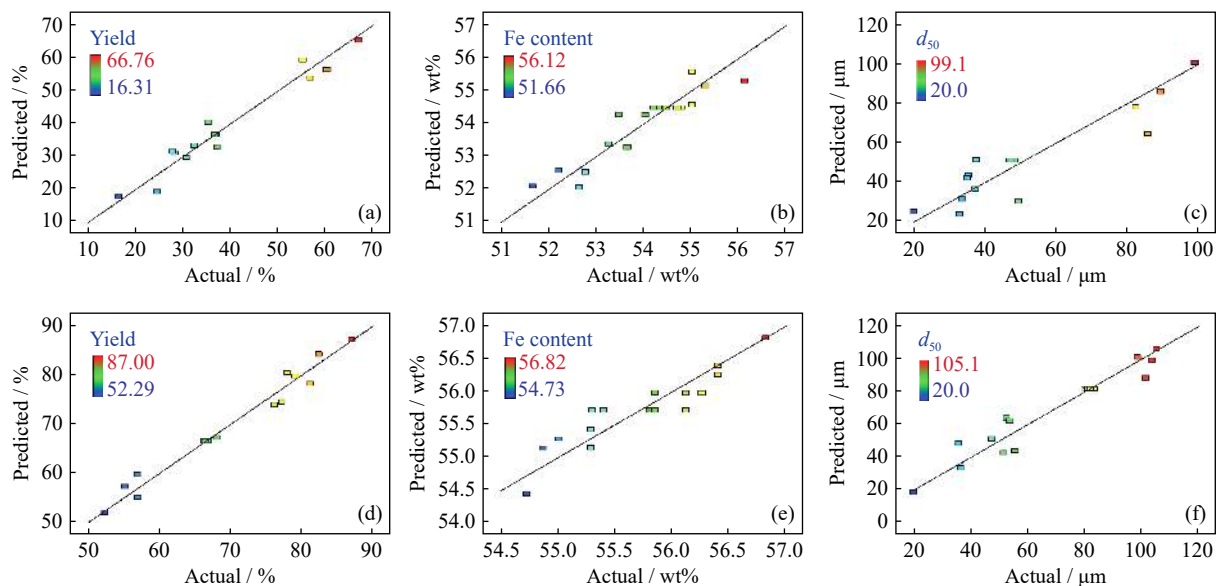


Fig. 5. Predicted vs. actual plots of all the models developed: (a) yield of sample 1; (b) Fe content of sample 1; (c) d_{50} (μm) of sample 1; (d) yield of sample 2; (e) Fe content of sample 2; (f) d_{50} of sample 2.

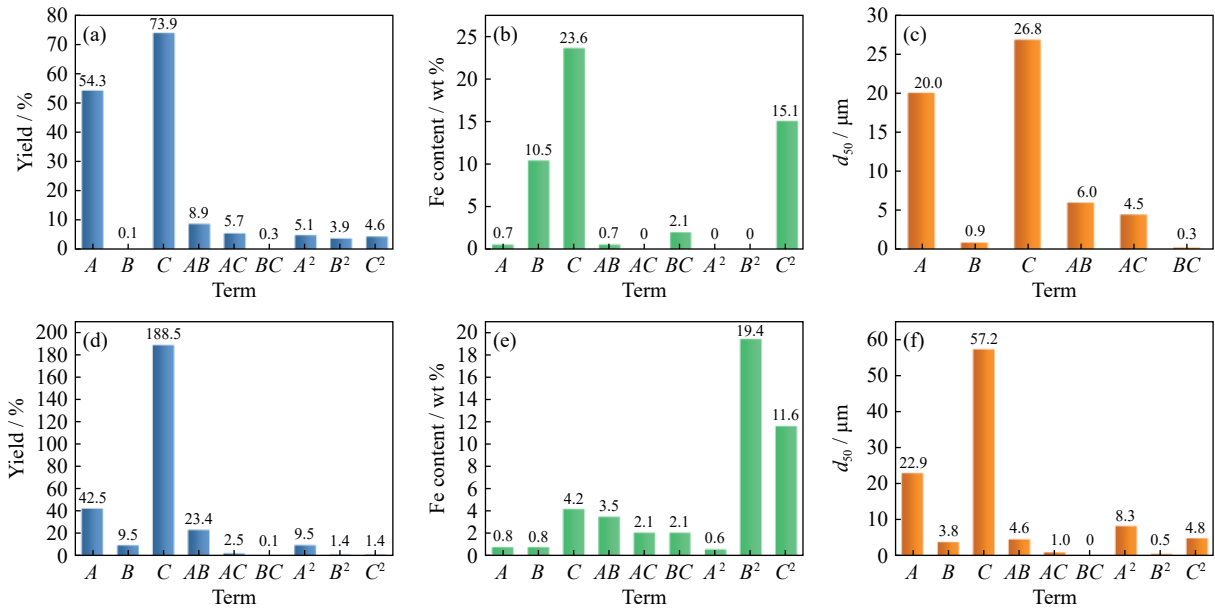


Fig. 6. *F* values of the different terms in equations: (a) Eq. (1), (b) Eq. (2), (c) Eq. (3), (d) Eq. (4), (e) Eq. (5), and (f) Eq. (6).

for Fe content (wt%). The *F* values of the different terms in the models developed for yield (%) and d_{50} show an almost similar trend in Samples 1 and 2. This can be attributed to the fact that yield (%) and d_{50} are directly related to each other. The results of the designed experiments presented in Table 6 suggest that the upgradation in Fe content is limited to 3%–5%, irrespective of the corresponding yield values. Therefore, the focus of the optimization study was to maximize the yield values.

The optimization study, carried out using the Nelder–Mead multidimensional pattern search technique, is presented pictorially in Fig. 7. Fig. 7(a) displays the 3D response surface plot of the yield of Sample 1 as a function of *A* and *B*,

while *C* has been considered as the actual factor. A maximum yield value of 40.60% is flagged at the optimum conditions, such as a feed rate of 839.88 kg/min, a cage wheel speed of 1080 r/min, and a blower speed of 34.40 r/min. The corresponding Fe grade, recovery, and d_{50} are predicted to be 55.35%, 43.78%, and 48.49 μm , respectively. Similarly, the data presented in Fig. 7(b) suggests that a maximum yield value of 85.24% can be obtained at a feed rate of 1800 kg/min, a cage wheel speed of 1080 r/min, and a blower speed of 25.35 r/min, for Sample 2. At these conditions, Sample 2 is predicted to generate a product having 56.59wt% Fe with an Fe recovery of 90.55% and d_{50} of 20 μm .

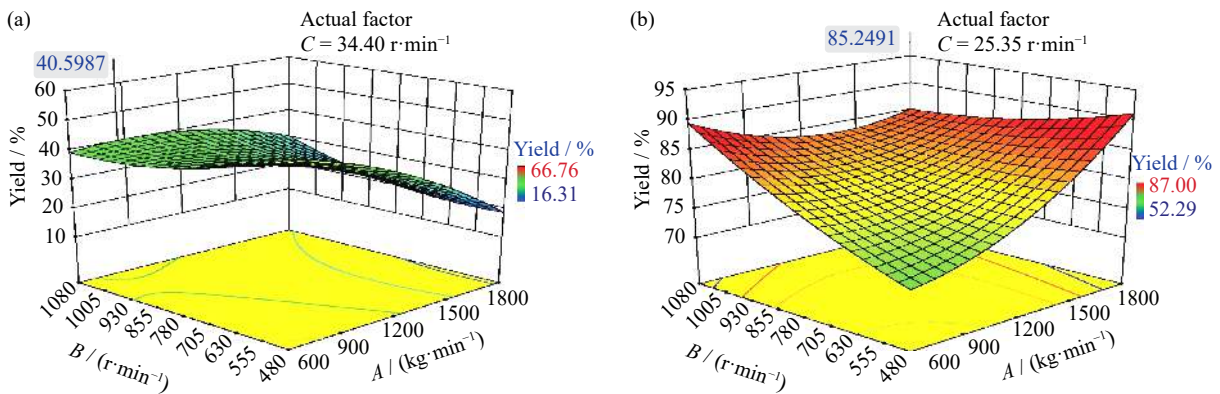


Fig. 7. 3D response surface plots for optimizing yield of (a) Sample 1 and (b) Sample 2.

3.3. Validation of the statistical optimization and product characterization

The optimized conditions for both samples are summarized in Table 8. The results of the optimization study were verified by carrying out three experiments at the suggested optimum levels, and the average reading was considered as the experimental value for the confirmatory test (Table 9). The corresponding yield, Fe content, and d_{50} values at the op-

timized conditions showed a good match with the predicted values since the estimated errors were below 5%.

Table 8. Optimum values of various statistical factors for both the samples

Sample No.	<i>A</i> / (kg·min ⁻¹)	<i>B</i> / (r·min ⁻¹)	<i>C</i> / (r·min ⁻¹)
1	839.88	1080	34.47
2	1800	1080	25.35

Table 9. Results of the confirmatory experiments at the optimized conditions for both the samples

Result	Sample 1			Sample 2		
	Yield / %	Fe content / wt%	d_{50} / μm	Yield / %	Fe content / wt%	d_{50} / μm
Predicted value by model	40.60	55.35	48.49	85.24	56.59	20.00
Experimental value	41.52	54.75	47.21	86.65	55.45	19.24
Error	2.27%	1.08%	2.64%	1.65%	2.01%	3.80%

The products obtained at the optimized process variables were also subjected to characterization, and the corresponding SEM images are shown in Fig. 8. The micrographs indicate that at optimized conditions, a slightly improved fines product could be obtained for Sample 1. On the other hand, the coarse product of Sample 2 at optimized process variables showed comparatively more iron phases, mostly hematite as liberated from the quartz phases. The iron oxide particles, comprising both hematite and goethite in Sample 2, range from a smaller size (10 μm) to a larger size of more than 100 μm in some cases. They occur as isolated patches and mostly in liberated form contributing towards the higher yield of Sample 2 than Sample 1, where the iron bearing phases (only hematite) are in very small size and also found associated with quartz.

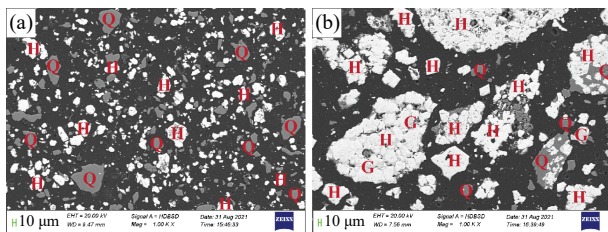


Fig. 8. SEM backscattered image of (a) fine product of Sample 1 and (b) coarse product of Sample 2 obtained at optimized process variables. H: Hematite, Q: Quartz, and G: Goethite.

As evident from the results of the statistical design, the maximum yield value of Sample 1 is obtained at a relatively lower feed rate and a higher blower speed compared to that of Sample 2. This phenomenon can be understood from the basic operating mechanism of a VSK separator. In a VSK separator, the feed material enters the V section, where primary classification takes place between the arrays of the cascading baffle plates arranged one over the other. Air enters transversely to the material flow, which carries the fine particles to the SK-cage wheel section. The coarse particles cascade over an array of plates and report to the bottom discharge. An increase in feed rate leads to a rise in the number of particles entering the V-section. Overcrowding of particles causes misplacement of a fraction of fines to the coarse product, thereby decreasing the yield to the fines product. The separation efficiency, i.e. the d_{50} cut size, decreases for the fines product. Thus, a low feed rate is preferable to obtain a higher yield of fines. As fines are the product in the case of Sample 1 and the coarse fraction is the product in the case of Sample 2, a lower feed rate is favourable for Sample 1, while a higher feed rate is essential to obtain a good yield in the case of Sample 2.

Furthermore, in the VSK separator, the transportation of particles from one to another section takes place under the influence of airflow. Hence, the blower speed plays a vital role in the VSK classification system. An increased blower speed increases the recovery of fine particles to the cyclone underflow. The yield and d_{50} cut size to the fines product increases with the increase in blower speed. This explains why a higher blower speed ends up with a better yield in the case of Sample 1, while Sample 2 requires a relatively lower blower speed. However, the literature pertaining to influence of the cage wheel speed on the separation behaviour of particles in the VSK separator is limited [13,25–26]. After classification in the V-section (static classification), the fine particles report to the SK-cage wheel section (dynamic classification). An increased cage wheel speed develops a negative pressure in the vicinity, increasing the suction of fine particles otherwise reported to the coarse product. The cage wheel speed increases yield and d_{50} cut size to the fines product. However, in the present study, cage wheel speed has a minimal role in deciding the yield of both the samples.

3.4. Partition curves

Partition curves are an indicator of the performance of any classification unit. They correlate the percentage of feed material of a particular size fraction that actually report to the underflow product. The slope steepness of the partition curve is an indicator of the sharpness of separation. These curves utilize the particle size distribution data of feed, coarse and fines product fractions to calculate the selectivity efficiency of an air classifier. The separation efficiency is defined as the amount of a particular size fraction ‘ i ’ of the feed material reporting either to the coarse or fines product, and is expressed as follows:

$$\text{Efficiency (\%)} = \frac{M_f}{M_c + M_f} \times 100\% \quad (7)$$

where M_f and M_c are the weights of the fines and coarse products at a particular size fraction ‘ i ’, respectively.

In this context, partition curves were constructed to evaluate the separation efficiency of VSK separator, for both the samples. The partition curves presented in this section are representative ones, which are constructed using a selected set of experimental data. They were drawn by considering the actual material being subjected to classification after correcting the air split in the bypass fraction. Fig. 9 is a characteristic curve (d_{50} cut-size) of the VSK separator that represents the separation efficiency while treating Sample-1. The slope steepness of the partition curve is an indicator of the sharpness of separation. The closer the slope of partition curve to the vertical axis, the higher the efficiency of separation. It can

be observed from the figure that an increase in particle size decreases the efficiency of fine particles reporting to the overflow product. The coarse particles having a particle size greater than 100 μm were also reporting to the fines product. The d_{50} cut-size varied between 25 and 82 μm . The partition curves presented in Fig. 10 show that the efficiency of coarse particles reporting to the underflow product increases with the increase in particle size. It can be observed from the figure that fine particles of about 20–30 μm were reporting to the coarse product, and d_{50} cut-size varies between 24 to 86 μm .

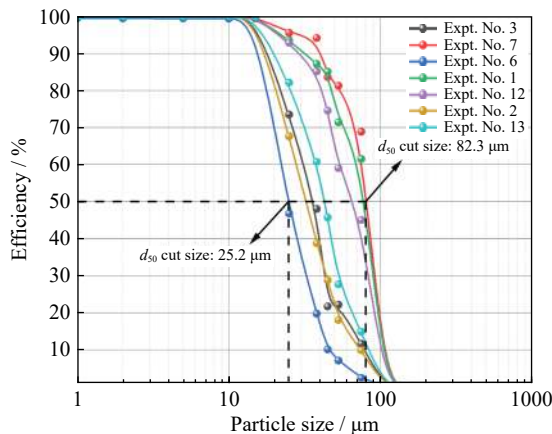


Fig. 9. Separation efficiency curves of VSK separator treating Sample 1.

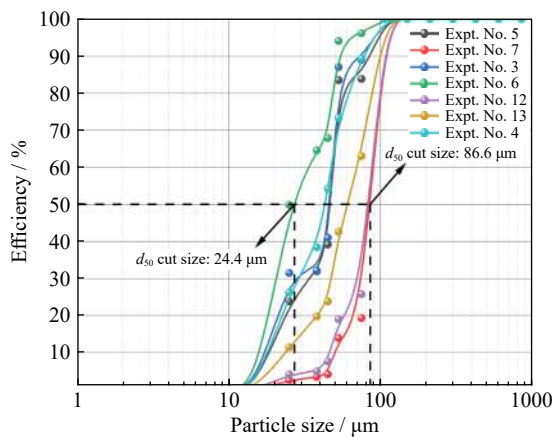


Fig. 10. Separation efficiency curves of VSK separator treating Sample 2.

4. Conclusion

In this study, the separation performance of two mineralogically different iron ores was evaluated using the statistical analysis of the designed experimental data and optimizing the process variables in a VSK separator. The mineralogy study indicated a possibility of separating the liberated iron minerals into the fines and the coarse products of Sample 1 and Sample 2, respectively. The statistical analysis revealed that a relatively lower feed rate and a higher blower speed are needed to maximize the fines content recovery. On the other hand, the cage wheel speed has a minimal impact on the separation performance. Under optimum conditions, from

Sample 1 containing ~51wt% Fe, it was possible to achieve fines product with ~55wt% Fe at a yield and a cut size of ~40wt% and 48 μm , respectively. Similarly, a coarse product having ~56wt% Fe could be obtained for Sample 2, having 53wt% Fe, at a yield of ~85wt% and a size cut of 20 μm . The results of the study recommend that VSK separator can be employed as an efficient dry classifier for such low-grade iron ore fines. However, it can be used as an intermediate unit operation, the product of which needs to be subjected to another unit for obtaining the final concentrate. Nevertheless, it saves a lot of water that is required for any wet classification unit.

Acknowledgement

The authors are thankful to the National Mineral Development Corporation Limited, Hyderabad for sponsoring the research and the Director, CSIR-Institute of Minerals and Materials Technology, Bhubaneswar for giving his consent to publish this work.

Conflict of Interest

The authors declare that they have no known competing financial interests or personal relationships that could have appeared to influence the work reported in this paper.

References

- [1] U.S. Geological Survey, *Mineral Commodity Summaries 2021*, U.S. Geological Survey, Reston, 2021, p. 200.
- [2] N. Ray, D. Nayak, N. Dash, and S.S. Rath, Utilization of low-grade banded hematite jasper ores: Recovery of iron values and production of ferrosilicon, *Clean Technol. Environ. Policy*, 20(2018), No. 8, p. 1761.
- [3] S.K. Roy, D. Nayak, and S.S. Rath, A review on the enrichment of iron values of low-grade Iron ore resources using reduction roasting-magnetic separation, *Powder Technol.*, 367(2020), p. 796.
- [4] S.S. Rath, H. Sahoo, and B. Das, Optimization of flotation variables for the recovery of hematite particles from BHQ ore, *Int. J. Miner. Metall. Mater.*, 20(2013), No. 7, p. 605.
- [5] S. Mahiuddin, S. Bondyopadhyay, and J.N. Baruah, A study on the beneficiation of Indian iron-ore fines and slime using chemical additives, *Int. J. Miner. Process.*, 26(1989), No. 3-4, p. 285.
- [6] M.P. Srivastava, S.K. Pan, N. Prasad, and B.K. Mishra, Characterization and processing of iron ore fines of Kiriburu deposit of India, *Int. J. Miner. Process.*, 61(2001), No. 2, p. 93.
- [7] H.J. Haselhuhn, J.J. Carlson, and S.K. Kawatra, Water chemistry analysis of an industrial selective flocculation dispersion hematite ore concentrator plant, *Int. J. Miner. Process.*, 102-103(2012), p. 99.
- [8] P. Dixit, D. Makhija, A.K. Mukherjee, V. Singh, A. Bhatnagar, and R.K. Rath, Characterization and beneficiation of dry iron ore processing plant reject fines to produce sinter/pellet grade iron ore concentrate, *Min. Metall. Explor.*, 36(2019), No. 2, p. 451.
- [9] K. Tudu, S. Pal, and N.R. Mandre, Comparison of selective flocculation of low grade goethitic iron ore fines using natural and synthetic polymers and a graft copolymer, *Int. J. Miner. Metall. Mater.*, 25(2018), No. 5, p. 498.

- [10] G. Jimbo, M. Yamazaki, J. Tsubaki, and T.S. Suh, Mechanism of classification in a sturtevant-type air classifier, *Chem. Eng. Commun.*, 34(1985), No. 1-6, p. 37.
- [11] S.K. Tripathy, P.K. Banerjee, N. Suresh, Y.R. Murthy, and V. Singh, Dry high-intensity magnetic separation in mineral industry—A review of present status and future prospects, *Miner. Process. Extr. Metall. Rev.*, 38(2017), No. 6, p. 339.
- [12] V. Nunna, S. Hapugoda, S.G. Eswarappa, S.K. Raparla, M.I. Pownceby, and G.J. Sparrow, Evaluation of dry processing technologies for treating low grade lateritic iron ore fines, *Miner. Process. Extr. Metall. Rev.*, 43(2022), No. 3, p. 283.
- [13] T. Kundu, S.K. Das, S.K. Tripathy, and S.I. Angadi, Performance evaluation of the VSK separator for treating mineral fines, *Miner. Eng.*, 167(2021), art. No. 106883.
- [14] P.B. Fu, Y.L. Fang, L. Ma, X. Jiang, Y. Liu, W.J. Lv, Y. Huang, L. Wang, J.P. Li, and H.L. Wang, Air acceleration classification for the enhancement of spent catalyst activity classification, *Sep. Purif. Technol.*, 223(2019), p. 31.
- [15] K. Heiskanen, *Particle Classification*, Chapman and Hall, London, 1993.
- [16] R. Srinivasan and V. Singh, Physical properties that govern fiber separation from distillers dried grains with solubles (DDGS) using sieving and air classification, *Sep. Purif. Technol.*, 61(2008), No. 3, p. 461.
- [17] R.A. Kleiv, Value enhancement of olivine process dust through air classification, *Int. J. Miner. Metall. Mater.*, 19(2012), No. 3, p. 185.
- [18] O. Altun and H. Benzer, Selection and mathematical modelling of high efficiency air classifiers, *Powder Technol.*, 264(2014), p. 1.
- [19] L. Karunakumari, C. Eswaraiah, S. Jayanti, and S.S. Narayanan, Experimental and numerical study of a rotating wheel air classifier, *AIChE J.*, 51(2005), No. 3, p. 776.
- [20] C. Eswaraiah, S.S. Narayanan, and S. Jayanti, A reduced efficiency approach-based process model for a circulating air classifier, *Chem. Eng. Process.: Process. Intensif.*, 47(2008), No. 9-10, p. 1887.
- [21] J. Muscolino, Mechanical centrifugal: Air classifiers, *Chem. Eng.*, 117(2010), No. 12, p. 48.
- [22] H. Li, Y.Q. He, J.S. Yang, X.N. Zhu, Z. Peng, and J.D. Yu, Segregation of coal particles in air classifier: Effect of particle size and density, *Energy Sources Part A*, 40(2018), No. 11, p. 1332.
- [23] W.H. Duda, *Cement Data Book: International Process Engineering in the Cement Industry*, 3rd Edition, French & European Pubns, 1985.
- [24] S. Routray and R.B. Rao, Classification studies in an advanced air classifier, *J. Inst. Eng. India Ser. D*, 97(2016), No. 2, p. 129.
- [25] T. Laxmi and B. Rao, Beneficiation studies on Teri sands, Tamilnadu by using advanced air cyclone classifier, *J. Min. Metall. Sect. A*, 50(2014), No. 1, p. 37.
- [26] F.P. van der Meer, Feasibility of dry high pressure grinding and classification, [in] *SAG Conference 2011*, Vancouver, 2011.
- [27] O. Altun, H. Benzer, H. Dundar, and N.A. Aydogan, Comparison of open and closed circuit HPGR application on dry grinding circuit performance, *Miner. Eng.*, 24(2011), No. 3-4, p. 267.
- [28] A. Martínez-L, A. Uribe S, F.R. Carrillo P, J. Coreño A, and J.C. Ortiz, Study of celestite flotation efficiency using sodium dodecyl sulfonate collector: Factorial experiment and statistical analysis of data, *Int. J. Miner. Process.*, 70(2003), No. 1-4, p. 83.
- [29] N. Aslan, Modeling and optimization of Multi-Gravity Separator to produce celestite concentrate, *Powder Technol.*, 174(2007), No. 3, p. 127.
- [30] N. Aslan and Y. Cebeci, Application of Box–Behnken design and response surface methodology for modeling of some Turkish coals, *Fuel*, 86(2007), No. 1-2, p. 90.
- [31] R.C. Chaurasia and S. Nikkam, Beneficiation of low-grade iron ore fines by multi-gravity separator (MGS) using optimization studies, *Part. Sci. Technol.*, 35(2017), No. 1, p. 45.
- [32] R.C. Chaurasia and S. Nikkam, Optimization studies on a multi-gravity separator treating ultrafine coal, *Int. J. Coal Prep. Util.*, 37(2017), No. 4, p. 195.
- [33] S.K. Jena, N. Dash, and S.S. Rath, Effective utilization of lime mud for the recovery of potash from mica scraps, *J. Clean. Prod.*, 231(2019), p. 64.